Rapid aging and disassembly of actin filaments from two evolutionary distant yeasts

Ingrid Billault-Chaumartin[1#], Hugo Wioland[1], Audrey Guillotin[2], Alphée Michelot[2,3], Antoine Jégou[1#], Guillaume Romet-Lemonne[1#]

1 Université Paris-Cité, CNRS, Institut Jacques Monod, F-75013 Paris, France
2 Aix Marseille University, CNRS, IBDM, Turing Centre for Living Systems, Marseille, France
3 CNRS International Research Laboratory Bridging Mechanobiology and Medicine (IRL 3639 BMC), Mechanobiology Institute, National University of Singapore (NUS), 5A Engineering Drive 1, 117411, Singapore
Corresponding authors: ingrid.billault@ijm.fr; antoine.jegou@ijm.fr; romet@ijm.fr

Summary

Actin is an essential cytoskeletal protein that is extremely well conserved across the tree of life. Similarities and differences in the way actin from different species self-assembles into filaments inform our understanding of its evolution. However, this basic knowledge is largely incomplete. Here, we address this issue by systematically characterizing assembly kinetics for actin from two yeast species that are five hundred million years apart in evolution, *Saccharomyces cerevisiae* and *Schizosaccharomyces pombe*, and compare them to the well-studied actin from rabbit skeletal muscle from which they diverged a billion years ago. By monitoring individual actin filaments under controlled conditions, we accurately quantified their barbed end elongation from ATP-actin monomers, their disassembly in the ADP·Pi and ADP states, as well as the release of inorganic phosphate, which marks their aging. We find that, in the ATP state, both yeast actins behave strikingly like mammalian actin at filament barbed ends. In contrast, yeast actin filaments in both the ADP·Pi and the ADP states depolymerize several-fold faster than their mammalian counterparts, and they release inorganic phosphate over 20-fold faster. We show that the absence of methylation on histidine 73 largely accounts for this faster aging of yeast actin filaments. We also reveal differences between the actins of the two yeasts. In particular, ADP-actin filaments depolymerize faster and are mechanically more flexible in *Saccharomyces cerevisiae* compared to *Schizosaccharomyces pombe*. Our findings suggest that actins expressed across species possess more diverse and specialized biochemical characteristics than previously recognized.

Introduction

In living cells, actin filaments and actin-binding proteins (ABPs) form dynamic networks that support fundamental functions such as division, motility and polarity (Lappalainen et al., 2022; Pollard & Cooper, 2009). Filamentous actin (F-actin) results from the assembly of the monomeric, globular protein actin (G-actin) into polar filaments, with so-called barbed and pointed ends, the former being more dynamic. G-actin contains an ATP molecule which upon incorporation onto the filament quickly gets hydrolysed into ADP·Pi (Korn et al., 1987) The inorganic phosphate (Pi) is subsequently released, giving rise to ADP-actin. The 3 different nucleotide states of F-actin each have different assembly dynamics, both at the barbed and pointed end (Fujiwara et al., 2007; Pollard, 1986).

Actin is one of the most conserved proteins, ubiquitously expressed throughout the eukaryotic kingdom, and with homologs in Archaea (Gunning et al., 2015; Rodrigues-Oliveira et al., 2023). Some organisms, such as commonly studied yeasts, express only one actin gene. Others express multiple actin isoforms, such as mammals which typically have 6 different isoforms (Perrin & Ervasti, 2010) or plants which can express up to 21 distinct isoforms (Šlajcherová et al., 2012). The alpha-skeletal muscle actin isoform of rabbit (*Oc*ACTA1), or the 100% amino acid sequence-identical homolog from chicken, has become a standard in the field due to its high abundance in muscle and good purification yield (Spudich & Watt, 1971). Most of our knowledge on actin dynamics stems from *in vitro* studies using actin from this single gene.

In spite of actin being highly conserved, extrapolating results from *Oc*ACTA1 to other actin orthologs must be done with caution. Notably, heterologous actins are not systematically interchangeable (Boiero Sanders et al., 2022). For instance, substituting actin in *Saccharomyces cerevisiae* (*Sc*Act1) with other eukaryotic actins is lethal or leads to various defects *in vivo*. The severity of the phenotype correlates negatively with the degree of homology between the actins (Boiero Sanders et al., 2022). In particular, despite a 90% amino acid identity, the replacement of *Sc*Act1 with the *Schizosaccharomyces pombe* actin gene (*Sp*Act1) is not viable. Furthermore, within one given organism, different isoforms can support distinct functions and can exhibit distinct localizations (Boiero Sanders et al., 2020; Perrin & Ervasti, 2010; Šlajcherová et al., 2012).

The non-interchangeability of actins is certainly due in part to some ABPs being isoform-specific. For example, cofilin from *Leishmania major* does not bind to *Oc*ACTA1 filaments, in spite of Leishmania cofilin-actin filaments being strikingly similar to their mammalian counterparts (Kotila et al., 2022). Intrinsic differences in the assembly properties of actin isoforms likely contribute to their non-interchangeability as well. Such differences appear clearly as diverse actin isoforms are being studied. For example, actin filaments from Apicomplexan parasites, which are distant in evolution from mammals, turn over much faster due to faster disassembly rates and a higher critical concentration for assembly (Lu et al., 2019; Hvorecny et al., 2024). These intrinsic kinetic differences are key for our understanding of the actin cytoskeleton and its evolution, which is still very incomplete.

In that respect, the two distant yeasts *Saccharomyces cerevisiae* (*S. cerevisiae*) and *Schizosaccharomyces pombe* (*S. pombe*) are particularly interesting. They diverged from each other about half a billion years ago (Shen et al., 2020) and twice that long ago from metazoans (Dohrmann & Wörheide, 2017), thus probing an intermediate region in the eukaryotic tree. In addition, both have been used as model organisms for decades, are amenable to quick genetic manipulation and have well-characterized actin networks (Mishra et al., 2014; Kovar et al., 2011). While their actin assembly kinetics are known to differ from the standard *Oc*ACTA1, quantifications of reaction rates and systematic comparisons are lacking. For example, *Sc*Act1 and *Sp*Act1 filaments have been reported to assemble faster, but this feature is attributed to a more efficient filament nucleation, and elongation rates have not been measured (Buzan & Frieden, 1996; Ti & Pollard, 2011). Likewise, *Sp*Act1 and *Sc*Act1 filaments have been reported to release Pi rapidly, but no reaction rate has been measured (Ti & Pollard, 2011; Yao & Rubenstein, 2001).

Here, we aim to fill this gap, taking advantage of recent techniques for the production of actin (Hatano et al., 2018, 2020) and for the monitoring of their assembly dynamics at the single filament level (Jégou et al., 2011; Wioland et al., 2022) using a low fraction of fluorescently labeled nucleotides (Colombo et al., 2021). We find that, in spite of their evolutionary distance, the two yeasts share highly similar ATP-actin dynamics to mammalian skeletal muscle actin, but accelerated ADP·Pi and ADP-actin barbed end depolymerization rates, in addition to a strikingly accelerated Pi-release rate. The accelerated Pi-release rate is largely explained by the absence of histidine 73 methylation, which is ubiquitous in mammalian actins but absent in yeast actins.

Results

ATP-actin from *Saccharomyces cerevisiae* and *Schizosaccharomyces pombe* polymerize at the same rate as mammalian actin

Saccharomyces cerevisiae (*S. cerevisiae*) and *Schizosaccharomyces pombe* (*S. pombe*) have single actin genes (coding for the proteins *Sc*Act1 and *Sp*Act1, respectively) that share close amino acid sequence identity to the 6 mammalian actin genes, reflecting the exceptional conservation of the actin gene in general (Figure S1). In particular, they respectively share 87 and 89% amino-acid sequence identity with the α-skeletal muscle *Oryctolagus cuniculus* (rabbit) homolog, *Oc*ACTA1, used in most *in vitro* actin characterization studies (Figure 1A and Table 1). *Sc*Act1 and *Sp*Act1 are only slightly more similar to each other than they are similar to *Oc*ACTA1, with 90% amino-acid sequence identity. In spite of these strong similarities in sequence, substituting one ortholog for another is lethal *in vivo* (Boiero Sanders et al., 2022).

To study the actin polymerization properties of the two divergent yeast actins of *S. cerevisiae* and *S. pombe*, we took advantage of a recently developed system that allows for the expression of recombinant eukaryotic actins in *Pichia pastoris* (Hatano et al., 2018, 2020). We purified both actins using this system in the presence of the N-terminal acetylation and in the absence of histidine 73 methylation, as is the case *in vivo* (Table 2). We monitored actin filaments using a low fraction of ATP-ATTO488 (Colombo et al., 2021), a method that is useful when the direct chemical labeling of actin is challenging, and that does not alter the rates at which filaments elongate (Colombo et al., 2021) and release Pi (Schahl et al., 2025). We then studied their barbed end polymerization kinetics by microfluidics-assisted TIRF microscopy (Figure 1B; Jégou et al., 2011; Wioland et al., 2022) at different actin concentrations. Experiments were carried out at 25°C, pH 7.4 (Methods). With this method, spectrin-actin seeds are anchored to the surface and the filaments grown from them are conveniently aligned by the flow (Figure 1C), easing the monitoring of their barbed end elongation over time (Figure 1D, movie S1). This allowed us to measure the elongation rate as a function of the concentration of actin monomers (Figure 1E).

At high actin concentrations, polymerization is fast enough to consider that the barbed end is mostly in the ATP state, and a linear fit yields the on- and off-rate constants (k_{on}^{ATP} and k_{off}^{ATP}) of ATP-actin at the barbed end (Figure 1E). Strikingly, these reaction rates for *Sp*Act1 and *Sc*Act1 are very similar to those published for *Oc*ACTA1 (Figure 1E, Table 3; Pollard, 1986; Jégou et al., 2011) with k_{on} = 11.6±0.7, 10.0±0.7 and 11.6±1.2 $\mu M^{-1}\ s^{-1}$, respectively, and k_{off} = 1.5±0.5, 1.0±0.5 and 1.4±0.8 s^{-1}, respectively. To our knowledge, these rate constants have not been previously measured, but our results are consistent with earlier studies in bulk assays on *S. cerevisiae* where faster polymerization was observed but attributed to nucleation rather than elongation (Buzan & Frieden, 1996), and bulk assays on *S. pombe* actin where elongation rates were not quantified but proposed to be similar to that of mammalian actin (Takaine & Mabuchi, 2007; Ti & Pollard, 2011).

Taken together, these results show that the two divergent yeasts *S. cerevisiae* and *S. pombe* share nearly identical ATP-actin barbed end dynamics to each other and to the well-studied metazoan actins. This was far from expected, since a single point mutation on an actin isoform is enough to greatly alter its elongation rate (Greve et al., 2024). In spite of their nearly identical rate constants, we found that these actin orthologs were

not fully interchangeable: mixing equal volumes of *Oc*ACTA1/*Sp*Act1, *Oc*ACTA1/*Sc*Act1, or *Sp*Act1/*Sc*Act1 solutions resulted in filaments elongating 13-19% slower than from the unmixed orthologs (Figures 1G-I and S2A-B). However, filaments made with actin from two different species did not appear to be more fragile (Figure S2C-D).

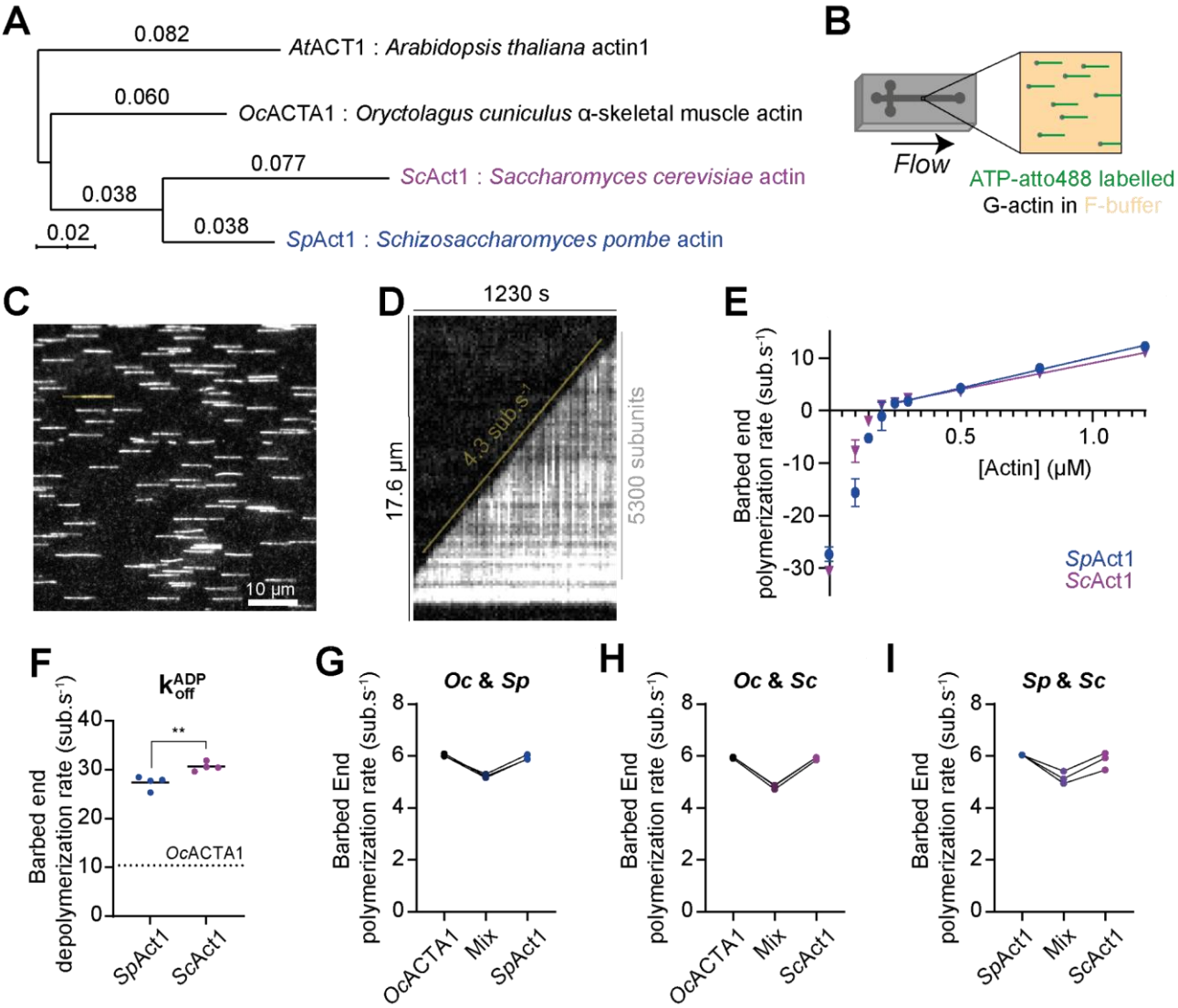

Figure 1. *Saccharomyces cerevisiae* and *Schizosaccharomyces pombe* actins exhibit indistinguishable ATP-actin dynamics from rabbit skeletal muscle actin but faster ADP-actin depolymerization rates.

A. Phylogenetic tree of the 3 actins used in this study, *Saccharomyces cerevisiae* actin *Sc*Act1 (Uniprot P60010), *Schizosaccharomyces pombe* actin *Sp*Act1 (Uniprot P10989) and *Oryctolagus cuniculus* (rabbit) alpha skeletal muscle actin *Oc*ACTA1 (Uniprot P68135). *Arabidopsis thaliana* actin 1 *At*ACT1 (Uniprot P0CJ46) was used as an external group. Scale bar unit is the average number of substitutions per amino-acid. **B.** Method used to study the dynamics of actin filaments in TIRF-assisted microfluidics experiments. ATP-atto488 G-actin (green) is flowed into a PDMS microfluidic chamber and polymerized in F-buffer (yellow) onto spectrin-actin seeds (grey) adsorbed onto the surface. This results in filaments anchored to the surface by their pointed end and whose dynamic barbed end can be monitored using TIRF microscopy. **C.** Example of a cropped field of view obtained with the method sketched in B using 0.5 µM *Sp*Act1 and 0.25 µM ATP-atto488. Movie S1 shows this cropped field of view over the course of the experiment. **D.** Kymograph of the filament outlined in C (yellow line) over the course of the acquisition. The elongation rate is obtained from the angle formed by the line following the filament barbed end over time (yellow line) and the abscissa. **E.** Plot of the barbed end polymerization rate as a function of the actin concentration for both *Sp*Act1 (blue) and *Sc*Act1 (magenta). Each point is the mean of at least 4 independent experiments where the elongation rate of 30 filaments was quantified as in D, and error

bars are standard deviations. A linear regression for points from 0.25 µM to 1.2 µM actin was used to extract k_{on}^{ATP} as the slope and k_{off}^{ATP} as the y-intercept (Table 3). **F.** The rates k_{off}^{ADP} correspond to the values at 0 µM actin in E (Table 3), measured after polymerizing the filaments. Each point is the mean of an independent replicate, and black bars are means of the replicates for a given condition. Dotted line is the value obtained for *Oc*ACTA1 in Wioland et al., 2019, for reference. Indicated significance is from an unpaired student t-test. (** : p≤0.01). **G-I.** Plots of the barbed end polymerization rate for pure solutions of *Oc*ACTA1 (black – G and H), *Sp*Act1 (blue – G and I), *Sc*Act1 (magenta – H and I) and their 50/50 respective mixes. Please note that the pure and mixed solutions are polymerized simultaneously in these experiments (see Figure S2A) to ensure identical experimental conditions. Each point is the mean of an independent replicate where the polymerization rate of 30 filaments was quantified, and points across categories stemming from the same acquisition are linked.

Actin filaments from *Saccharomyces cerevisiae* and *Schizosaccharomyces pombe* disassemble much faster than mammalian actin filaments

At low actin concentrations, we found that *Sp*Act1 and *Sc*Act1 filaments depolymerized rapidly and at similar rates (Figure 1E). In this regime, the addition of subunits to the barbed end is less frequent than the rate of ATP hydrolysis in F-actin (0.3 s^{-1} for rabbit skeletal muscle actin; Blanchoin & Pollard, 2002) and the terminal subunits can be in different nucleotide states. In the absence of G-actin in solution, filaments reach a steady-state where they depolymerize as ADP-actin, at a rate k_{off}^{ADP}. We found that the two yeast actins used in this study depolymerized roughly 3-fold faster than what is reported for rabbit alpha-skeletal actin: k_{off}^{ADP} = 27.4±1.4 and 30.6±0.9 s^{-1} for *Sp*Act1 and *Sc*Act1, respectively (Figure 1E-F, Table 3), compared to 10.4±0.5 s^{-1} for *Oc*ACTA1 in the same conditions (Wioland et al., 2019).

We next sought to investigate the depolymerization rate of *S. cerevisiae* and *S. pombe* ADP·Pi-actin. The ADP·Pi-actin situation is more complex because the barbed end subunit is known, at least in mammalian actin, to release its inorganic phosphate (Pi) far more rapidly than subunits within the filament (Jégou et al., 2011; Oosterheert et al., 2023). As a consequence, an ADP·Pi-actin filament depolymerizes at a rate $v_{ADP\cdot Pi}$ which combines two routes, as subunits can either dissociate as ADP·Pi-actin at a rate $k_{off}^{ADP\cdot Pi}$, or release their Pi and then dissociate as ADP-actin at a rate k_{off}^{ADP} (Fig S3). In order to determine $k_{off}^{ADP\cdot Pi}$, one can force dissociation to follow the first route. To do so, we polymerized filaments in phosphate buffer, then switched to the same phosphate buffer condition without actin (Figure 2A-B, movie S2). The higher the concentration of Pi, the closer the barbed end subunits are to being fully in the ADP·Pi state, and the depolymerization rate eventually plateaus at $k_{off}^{ADP\cdot Pi}$ when all subunits dissociate as ADP·Pi-actin (Figure 2C). For both yeast actins, we used the depolymerization rate at 200 mM phosphate as an estimate of this plateau value, yielding $k_{off}^{ADP\cdot Pi}$ = 6.39±0.93 and 2.73±0.13 s^{-1} for *Sp*Act1 and *Sc*Act1, respectively (Figure 2D, Table 3). These values are significantly different and, compared to *Oc*ACTA1 (0.16±0.07 s^{-1}; Jégou et al., 2011), about 40-fold faster for *Sp*Act1 and 17-fold faster for *Sc*Act1.

Changing the phosphate concentration has an effect on the ionic strength of the solution and on its ability to solubilize proteins (ion-specific, Hofmeister effects), which could themselves potentially affect the depolymerization rate. To control for these possible effects, we measured *Sp*Act1 and *Sc*Act1 depolymerization rates with increasing concentrations of KCl and with increasing concentrations of Na_2SO_4 (SO_4^{2-} being similarly kosmotropic as PO_4^{3-}, Mazzini & Craig, 2017). We found that they had a weak impact on both *Sp*Act1 and *Sc*Act1 (Figure S4A-B).

Taken together, these results show that ADP- and ADP·Pi-actin filaments for both *S. cerevisiae* and *S. pombe* depolymerize strikingly faster than for mammalian skeletal muscle actin.

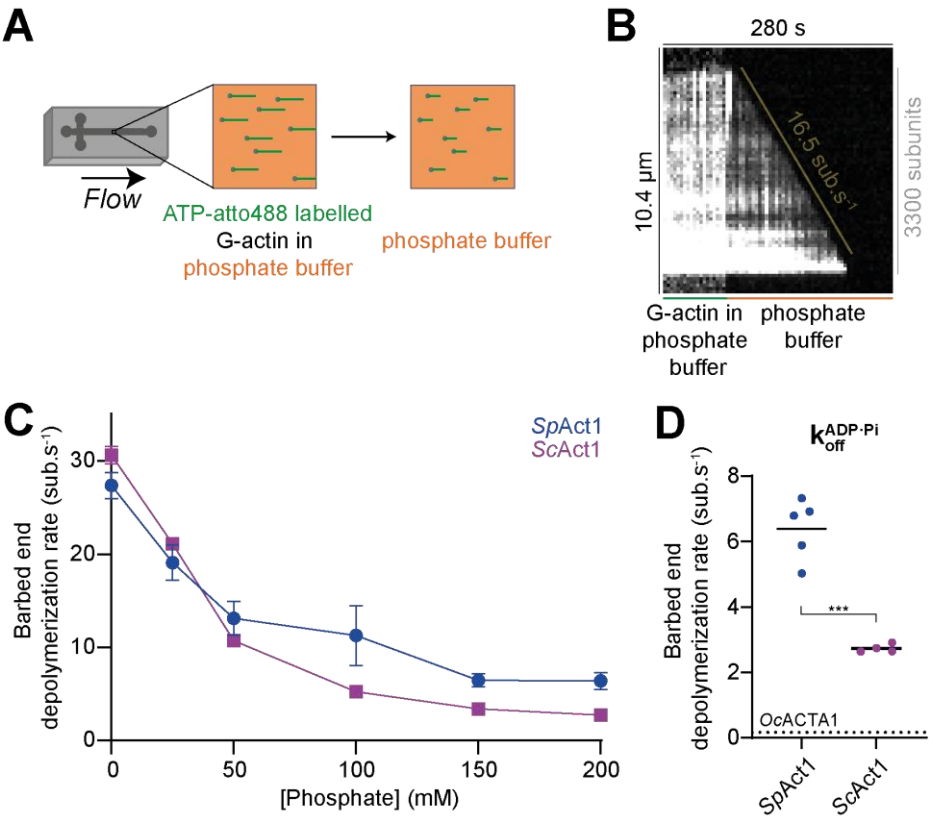

Figure 2. *Saccharomyces cerevisiae* and *Schizosaccharomyces pombe* ADP·Pi-actin filaments depolymerize fast.

A. Method used to study the depolymerization of ADP·Pi-actin filaments in TIRF-assisted microfluidics experiments. ATP-atto488 G-actin (green) is flowed into a PDMS microfluidic chamber and polymerized in phosphate-buffer (orange) onto spectrin actin seeds (grey). The filaments are then exposed to the same phosphate buffer without actin and their depolymerization is monitored. **B.** Kymograph of an actin filament over the course of an experiment as in A using 1µM *Sp*Act1, 0.5 µM ATP-atto488 and 25 mM phosphate (see Movie S2). **C.** Plot of the barbed end depolymerization rate as a function of the phosphate concentration for both *Sp*Act1 (blue) and *Sc*Act1 (Magenta). Each point is the mean of at least 4 independent experiments where the elongation rate of at least 15 filaments was quantified as in B and error bars are standard deviations. **D.** Depolymerization rates $k_{off}^{ADP \cdot Pi}$ correspond to data at 200µM phosphate in C (Table 3). Each point is the mean of an independent replicate, and black bars are means of the replicates for a given condition. Dotted line is the value obtained for *Oc*ACTA1 in Jégou et al., 2011, for reference. Indicated significance is from an unpaired student t-test (*** : p≤0.001)

Actin filaments from *Saccharomyces cerevisiae* and *Schizosaccharomyces pombe* release their inorganic phosphate much faster than mammalian actin filaments

An important aspect of actin dynamics is the transition from the ADP·Pi to the ADP state, which makes the filaments less stable and plays an important role in controlling the binding of regulatory proteins (Blanchoin & Pollard, 1999; Cai et al., 2007; Zimmermann et al., 2015). Hence, we next sought to investigate how fast yeast actins release their inorganic phosphate (Pi). For that, we polymerized filaments in phosphate buffer, as before, but then switched to a buffer without phosphate for depolymerization (Figure 3A). Because $k_{off}^{ADP \cdot Pi}$ is lower than k_{off}^{ADP}, we observed an increase of the depolymerization rate over time, as Pi is progressively released from actin subunits of the filament (Figure 3B). By analyzing this acceleration (Figure S9) we can extract the Pi-release rate k_r (Jégou et al., 2011; Kotila et al., 2022; Oosterheert et al., 2023; Methods).

We find that Pi release from F-actin is 23-fold faster for *S. pombe* and 86-fold faster for *S. cerevisiae*, compared to mammals: k_r = 0.16±0.06 s^{-1} and 0.58±0.13 s^{-1} for *Sp*Act1 and *Sc*Act1, respectively (Figure 3D, Table 3), compared to 0.0068±0.0021 s^{-1} for *Oc*ACTA1 (rate from (Jégou et al., 2011), in agreement with (Melki et al., 1996; Fujiwara et al., 2007; Oosterheert et al., 2023)). Pi release in the two yeast actins differs, as it is 4-fold faster for *Sc*Act1 than *Sp*Act1. Our 23-fold increase for *Sp*Act1 compared to *Oc*ACTA1 is consistent with earlier bulk assays which estimated a 10- to 100-fold increase, lacking in precision due to a limited temporal resolution (Ti & Pollard, 2011).

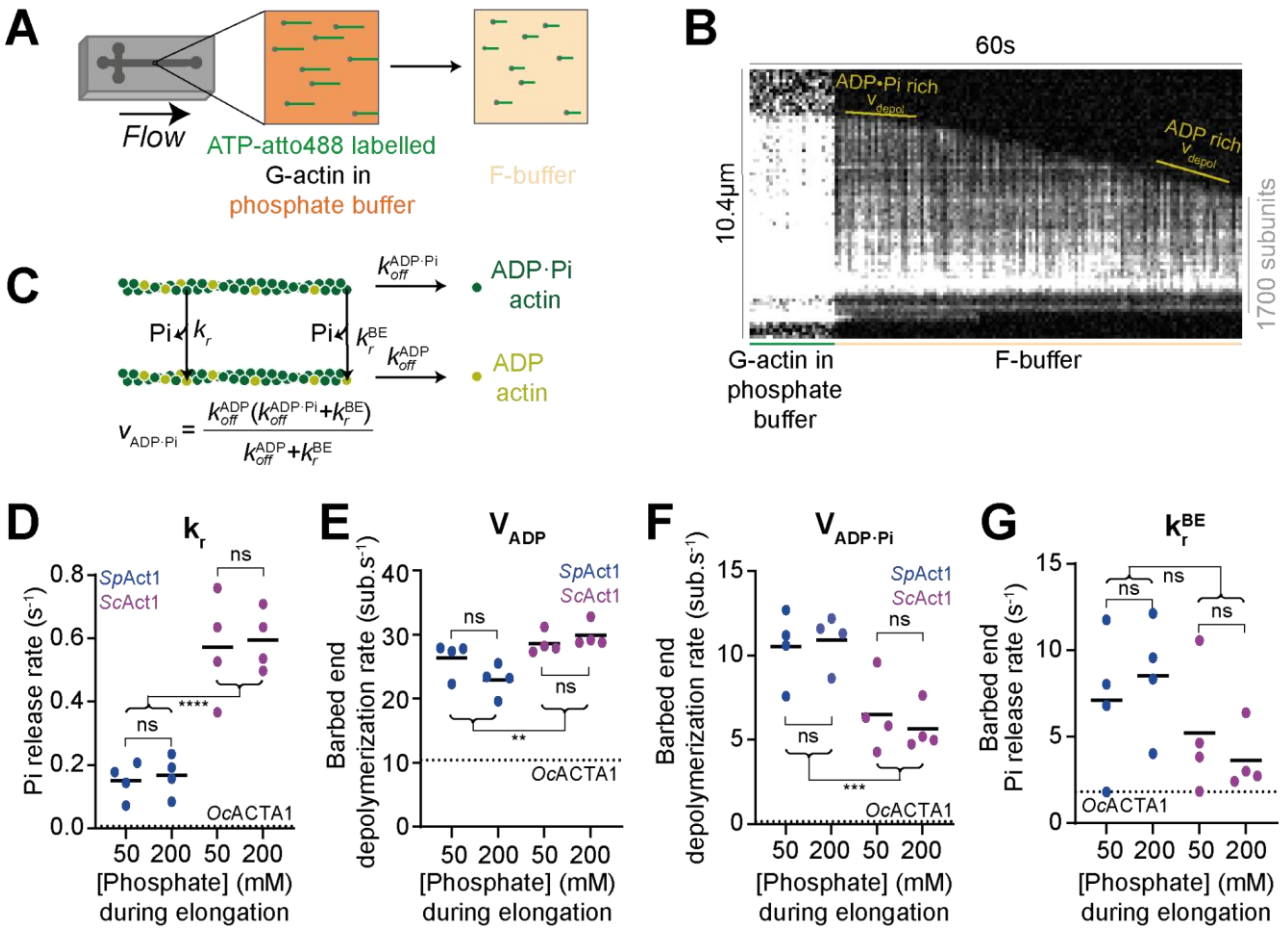

Figure 3. *Saccharomyces cerevisiae* and *Schizosaccharomyces pombe* actin filaments release inorganic phosphate faster than rabbit alpha-skeletal actin filaments.

A. Method used to study the phosphate release rate of actin filaments in TIRF-assisted microfluidics experiments. ATP-atto488 G-actin (green) is flowed into a PDMS microfluidic chamber and polymerized in phosphate-buffer (orange) onto spectrin actin seeds (grey). The filaments are then exposed to F-buffer (yellow) without actin and depolymerization is monitored over time. **B.** Example of a kymograph of an actin filament over the course of an experiment as in A using 0.8 µM *Sp*Act1, 0.4 µM ATP-atto488 and 50 mM phosphate. **C.** Scheme explaining the different rates measured in this experiment. The depolymerization rate $V_{ADP\cdot Pi}$ is in subunits per second. **D.** Plot of the phosphate release rate k_r for *Sp*Act1 (blue) and *Sc*Act1 (magenta) following a polymerization at 50 and 200 mM phosphate. **E.** Plot of the depolymerization rate V_{ADP} at the end of the experiment for *Sp*Act1 (blue) and *Sc*Act1 (magenta) following a polymerization at 50 and 200 mM phosphate. **F.** Plot of the depolymerization rate $V_{ADP\cdot Pi}$ at the beginning of the experiment for *Sp*Act1 (blue) and *Sc*Act1 (magenta) following a polymerization at 50 and 200 mM phosphate. **G.** Plot of the barbed end phosphate release rate k_r^{BE} for *Sp*Act1 (blue) and *Sc*Act1 (magenta) following a polymerization at 50 and 200 mM phosphate, calculated from $V_{ADP\cdot Pi}$ (F), $k_{off}^{ADP\cdot Pi}$ (Figure 2D) and k_{off}^{ADP} (Figure 1F) using the equation in C. Dotted line is the value obtained for *Oc*ACTA1 in Jégou et al., 2011 (D, F, G) or Wioland et al., 2019 (E), for reference. Each point is the result of the fit of the depolymerization rate curve extracted from at least 40 filaments. Black bars are means of the replicates for a given condition. Indicated significances are from unpaired student t-tests (ns : p>0.05 ; ** : p≤0.01 ; *** : p≤0.001 ; **** : p≤0.0001).

Analyzing the acceleration of depolymerization over time (Fig 3B, Methods) also yields the depolymerization rate of the ADP·Pi-actin filament, $V_{ADP\cdot Pi}$, corresponding to the beginning of the depolymerization, as well as the depolymerization rate of the ADP-actin filament, V_{ADP}, corresponding to later times when the actin subunits have all released their Pi. By definition, V_{ADP} is identical to k_{off}^{ADP}, and the values we find (24.6±3.0 s^{-1} for SpAct1 and 29.3±1.8 s^{-1} for ScAct1, Figure 3E) match our previous measurements of k_{off}^{ADP} (Figure 1F).

In contrast, $V_{ADP\cdot Pi}$ is faster than $k_{off}^{ADP\cdot Pi}$, as revealed previously for rabbit skeletal muscle actin (Jégou et al., 2011). This is because, as mentioned earlier (Figure S3), actin subunits at the barbed end release their Pi at a rate k_r^{BE}, faster than the rest of the filament. Thus, the depolymerization of ADP·Pi-actin can happen via two routes: (1) the ADP·Pi subunit dissociates from the barbed end as ADP·Pi-actin or (2) it first releases its Pi and then dissociates as ADP-actin (Figure 3C). We found that $V_{ADP\cdot Pi}$ is notably faster for *Sp*Act1 ($V_{ADP\cdot Pi}$ = 10.7±1.7 s^{-1}) than *Sc*Act1 ($V_{ADP\cdot Pi}$ = 6.1±1.8 s^{-1}, Figure 3F). Knowing $V_{ADP\cdot PI}$, $k_{off}^{ADP\cdot Pi}$ and k_{off}^{ADP}, we can compute k_r^{BE} which is indeed much faster than k_r (Figure 3G, Table 3). We find that k_r^{BE} is almost twice as fast for *Sp*Act1 (7.8±4.1 s^{-1}) than for *Sc*Act1 (4.4±2.9 s^{-1}), though with a weak statistical significance ($p = 0.0554$), and both are markedly faster than for *Oc*ACTA1 (1.8±0.6 s^{-1}).

To verify that the actin filaments were indeed fully in the ADP·Pi state when switching to depolymerizing conditions, we repeated the experiment with different concentrations of phosphate buffer. Whether the filaments were polymerized in the presence of 50 or 200 mM phosphate, we found no significant difference in the rates we extracted from their subsequent depolymerization (Figure 3D-G). This result indicates that the bulk of the filament is already saturated with Pi at 50 mM (unlike the barbed end, Figure 2C), and validates our assay.

Together, these results show that *S. pombe* and *S. cerevisiae* actin filaments have faster Pi-release rates than mammalian actin filaments, both from subunits inside the filament and at the barbed end.

The faster Pi-release rate of yeast actins is largely due to the absence of histidine 73 methylation

We next sought to determine why the Pi-release rates of *Sc*Act1 and *Sp*Act1 are faster than for *Oc*ACTA1. An appealing hypothesis is the known absence of the histidine 73 methylation in yeast, an essential and ubiquitous post-translational modification (PTM) in metazoan actins (Figure 4A, Table 2), whose removal from β rabbit actin was recently shown to accelerate Pi release (Schahl et al., 2025). In *S. cerevisiae*, mutations of histidine 73 were shown to affect actin assembly *in vitro* (Yao et al., 1999) and recent high-resolution cryoEM structure suggests that the hydrogen bonds in the vicinity of histidine 73 may affect Pi release (Stevenson et al., 2025).

To test this hypothesis directly for *S. pombe*, we expressed *Sp*Act1 in a *Pichia pastoris* strain expressing SETD3, the enzyme responsible for the histidine 73 methylation in mammalian actins (Wilkinson et al., 2019). Using mass spectrometry, this was shown to produce actin that is 100% methylated on histidine 73 (Hatano et al., 2020). Similarly, using mass spectrometry, we validated that the vast majority of our SpAct1 recombinantly expressed in the presence of SETD3 was methylated on histidine 73 (Figure S8). We refer to this actin as *Sp*Act1^{H73me}.

The resulting actin assembly dynamics for *Sp*Act1^{H73me} were then assessed in the same way as for *Sp*Act1 and *Sc*Act1. The kinetic rate constants we measured for ATP-actin at the barbed end, k_{on}^{ATP} = 11.7±0.7 $s^{-1}.\mu M^{-1}$ and k_{off}^{ATP} = 1.1±0.6 s^{-1}, were indistinguishable from those of both *Sp*Act1 and *Oc*ACTA1 (Figure 4B, Table 3). The barbed end off-rate constant of ADP-actin, k_{off}^{ADP} = 29.1±0.8 s^{-1}, was also not significantly different from the one of *Sp*Act1 and was similarly accelerated compared to *Oc*ACTA1 (Figure 4B, Table 3). However, *Sp*Act1^{H73me} barbed ends seemed to be saturated in phosphate slightly more easily than its non-methylated counterpart (Figure 4C) and displayed a lower ADP·Pi-actin off-rate, $k_{off}^{ADP\cdot Pi}$ = 2.8±0.1 s^{-1} (compared to 6.4±0.9

s^{-1} for non-methylated *Sp*Act1), which is still much faster than for *Oc*ACTA1 (Table3). The ionic effects were as negligible as for its non-methylated counterpart (Figure S4C).

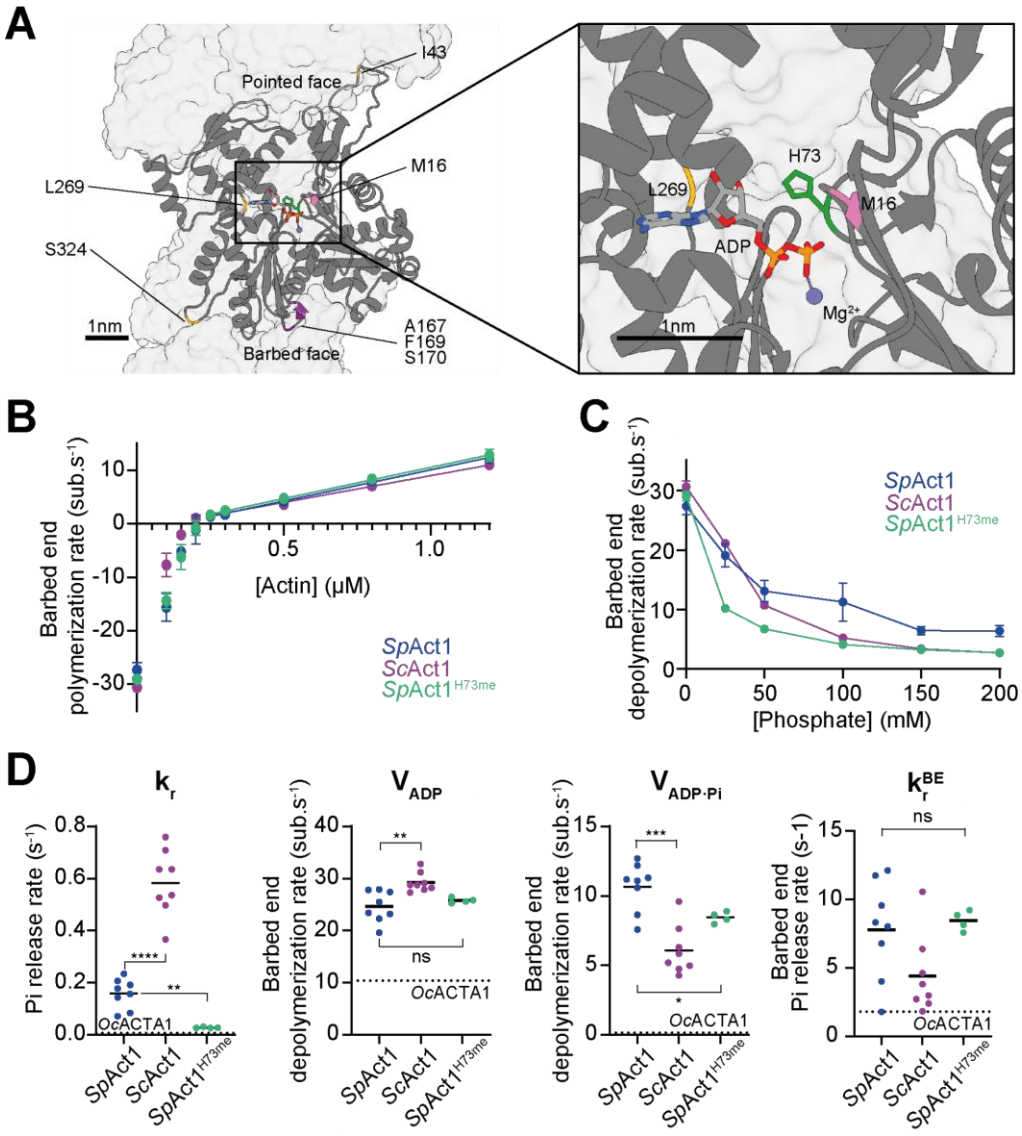

Figure 4. Histidine 73 methylation of *Schizosaccharomyces pombe* actin slows down Pi-release rate.

A. Backbone of an *S. cerevisiae* F-actin subunit (PDB 9go5, from Stevenson et al., 2025) within the filament. The unmethylated histidine 73 (H73) residue is highlighted in green. Methionine 16 (M16), in pink, is present in *S. cerevisiae*, *S. pombe* and beta/gamma mammalian actins, but is replaced by leucine 16 in mammalian alpha-skeletal actin. In yellow are residues isoleucine 43 (I43), leucine 269 (L269) and serine 324 (S324), which are the same in *S. pombe* and *S. cerevisiae*, but are changed to valine 43, methionine 269 and threonine 324 in alpha-skeletal, beta and gamma cytoplasmic actins in mammals. Located in the W-loop, residues alanine 167 (A167), phenylalanine 169 (F169) and serine 170 (S170) in *S. cerevisiae* differ from their counterparts in both *O. cuniculus* and *S. pombe* and are in Magenta. **B.** Plot of the barbed end polymerization rate as a function of the actin concentration for *Sp*Act1^{H73me} (Green). Values for *Sp*Act1 (Blue) and *Sc*Act1 (Magenta) are a duplicate of Figure 1E and are added for reference. Each point is the mean of at least 4 independent experiments where the elongation rate of 30 filaments was quantified and error bars are standard deviation. A linear regression for points from 0.25 µM to 1.2 µM actin was used to extract k_{on}^{ATP} as the slope and k_{off}^{ATP} as the -Y interception (Table 3). The values at 0 µM actin give the k_{off}^{ADP} (Table 3). **C.** Plot of the barbed end depolymerization rate as a function of the phosphate concentration for *Sp*Act1^{H73me} (Green). Values for *Sp*Act1 (Blue) and *Sc*Act1 (Magenta) are a duplicate of Figure 2C and are added for reference. Each point is the mean of at least 4 independent experiments where the elongation rate of at least 15 filaments was quantified, and error bars are standard deviation. Data at 200 µM phosphate was used for $k_{off}^{ADP\cdot Pi}$ (Table 3). **D.** Plots of the phosphate release rate k_r, the depolymerization rate V_{ADP}, the

depolymerization rate $V_{ADP\cdot Pi}$ and the barbed end phosphate release rate k_r^{BE}, for *Sp*Act1 (blue), *Sc*Act1 (magenta) and *Sp*Act1^{H73me} (Green). Data for *Sp*Act1 and *Sc*Act1 are pooled data from Figure 3D-G included for comparison. Because polymerizing at 50 or 200 mM phosphate had no impact for *Sp*Act1 and *Sc*Act1, data for *Sp*Act1^{H73me} were extracted from experiments done at 50 mM exclusively. Dotted line is the value obtained for *Oc*ACTA1 in Jégou et al., 2011 (k_r, $V_{ADP\cdot Pi}$, K_r^{BE}) or Wioland et al., 2019 (V_{ADP}), for reference. Each point is the result of the fit of the depolymerization rate curve extracted from at least 40 filaments. Black bars are means of replicates for a given condition. Indicated significances are from unpaired student t-tests. (ns : p>0.05 ; * : p≤0.05 ; ** : p≤0.01 ; *** : p≤0.001 ; **** : p≤0.0001)

Interestingly, histidine 73 methylation reduces the Pi-release rate of *S. pombe* actin filaments approximately 6-fold: k_r = 0.028±0.002 s^{-1} for *Sp*Act1^{H73me}, compared to 0.16±0.06 s^{-1} for *Sp*Act1 (Figure 4D). Pi release for *Sp*Act1^{H73me} is still about 4-fold faster than for *Oc*ACTA1 (Jégou et al., 2011). Mammalian beta actin, which is closer to *Sp*Act1 in amino acid sequence identity than *Oc*ACTA1 (Figure S1), was reported to release Pi from filaments either at the same rate as *Oc*ACTA1 (Oosterheert et al., 2023) or 2.5-fold faster (Schahl et al., 2025) which would make it similar to *Sp*Act1^{H73me} in that respect. We found that Pi release from the barbed end was not significantly affected by histidine 73 methylation (Figure 4D).

Together, these results show that the absence of histidine 73 methylation accounts for most of the differences between *S. pombe* and mammalian actins in terms of Pi release from the filament, while it has little or no effect on the other rates we measured.

Yeast actin filaments are slightly more flexible than mammalian actin filaments

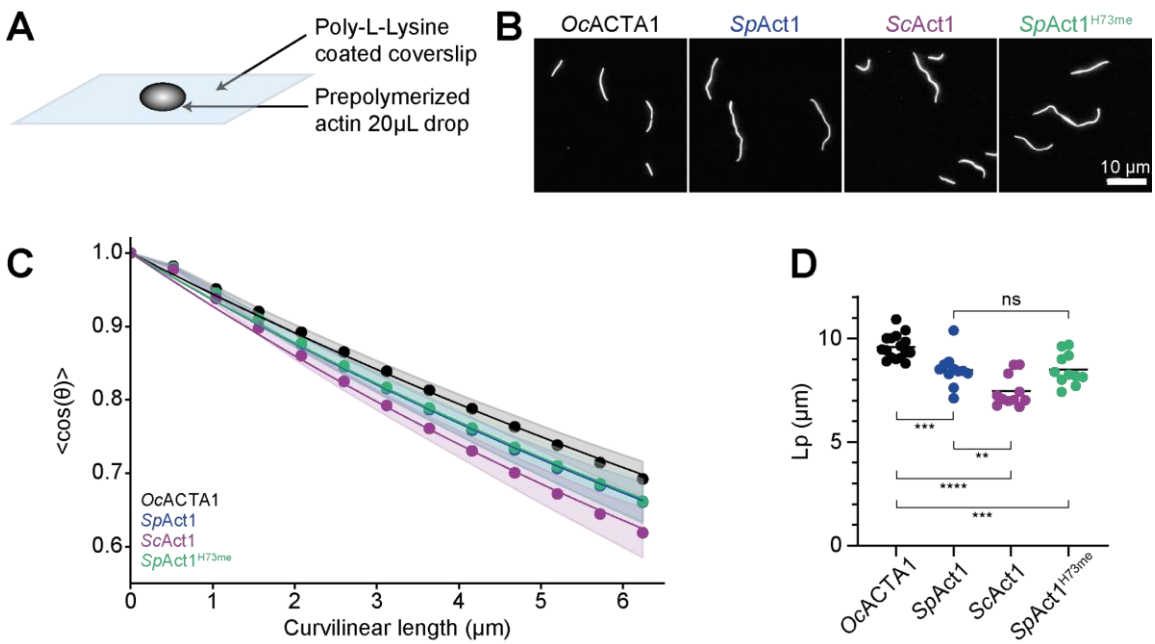

Figure 5. The persistence length of yeast actin filaments is reduced compared to rabbit actin independently of histidine 73 methylation.

A. Method used to study the persistence length of actin filaments. Pre-polymerized ATP-atto488 F-actin is deposited onto a coverslip functionalized with poly-L-lysine. Snapshots of surface-attached filaments are quickly recorded by fluorescence microscopy before the solution dries. **B.** Example of a field of view using the method in A for *Oc*ACTA1 (black), *Sp*Act1 (blue), *Sc*Act1 (magenta) and *Sp*Act1^{H73me} (Green). **C.** Average cosine angle correlation as a function of the curvilinear distance between two points along actin filaments for the different actins. Data points for each actin are the mean values from at least 11 independent experiments, each containing at least 323 filaments. Shaded areas are standard deviations.

Lines are exponential fits (see Methods). **D.** Plots of the persistence length for *Oc*ACTA1 (black), *Sp*Act1 (blue), *Sc*Act1 (magenta) and *Sp*Act1^{H73me} (Green). Each point is the result of the cosine correlation fit extracted from at least 323 filaments. Black bars are means of replicates for a given condition. Indicated significances are from unpaired student t-tests. (ns : p>0.05 ; ** : p≤0.01 ; *** : p≤0.001 ; **** : p≤0.0001)

The barbed end dissociation rate partly reflects the strength of the bonds between actin subunits within the filament, which has bearings on the mechanical stiffness of the filament. This made us wonder if *Sp*Act1 and *Sc*Act1 filaments were more flexible than *Oc*ACTA1 filaments. Previous literature indicates that *S. cerevisiae* actin filaments might be more flexible than their mammalian counterparts (Kang et al., 2012; X.-P. Xu et al., 2024; Stevenson et al., 2025; McCullough et al., 2011). We sought to confirm this and ask whether this property is conserved in yeast beyond *S. cerevisiae*. For that, we used a simple assay where we stick actin filaments to a coverslip coated with poly-L-lysine (Figure 5A) and determined their persistence Length Lp by fitting the average angular cosine correlation along filaments (Figure 5B-D, Methods). Interestingly, in our conditions, we found that *Sc*Act1 filaments, with Lp = 7.46±0.76 µm, were slightly but significantly more flexible than *Sp*Act1 filaments, for which Lp = 8.48±0.41 µm (Figure 5D). Both yeast actin filaments were more flexible than *Oc*ACTA1 filaments, for which we measured Lp = 9.59±0.59 µm. This decrease in persistence length was not rescued by the methylation of histidine 73, which did not seem to change the persistence length of *Sp*Act1 filaments (Figure 5D).

Discussion

By directly comparing *Schizosaccharomyces pombe* (*S. pombe*) and *Saccharomyces cerevisiae* (*S. cerevisiae*) actin filaments, we showed that they have strikingly similar assembly dynamics, in spite of their evolutionary distance. The two actins differ mildly in their kinetics of disassembly, and not in a systematic fashion: for example, the off-rate is higher for *S. pombe* in ADP·Pi-actin, and higher for *S. cerevisiae* in ADP-actin (Table 3). These reaction rate constants should prove valuable for studies that aim to understand the differences between actin-driven mechanisms in the two yeasts, such as endocytosis (Nickaeen et al., 2022; Picco et al., 2025). The two actins differ also in filament stiffness, *S. cerevisiae* actin filaments having a lower persistence length. Differences in amino acid composition likely account for the kinetic and mechanical differences that we measured. For example, the W loop, that mediates longitudinal contacts between subunits in the filament, contains residues which differ in the two yeasts (shown in magenta in Figure 4A) and could explain in part why *S. cerevisiae* actin filaments are more flexible (Stevenson et al., 2025; Figure 5). In fact, this residue difference seems specific to *S. cerevisiae* among known eukaryotic actins (Figure S1) suggesting that increased flexibility may be a feature of *S. cerevisiae*.

Compared to metazoan actins, and in particular the widely studied alpha-skeletal actin from rabbit, we found that actin from the two yeasts assembled equally fast: the reaction rate constants for ATP-actin at the barbed end were indistinguishable at 25°C. The identical on-rate constant k_{on}^{ATP} was not expected since it is not a necessary consequence of muscle ATP-actin barbed end elongation being diffusion-limited (Drenckhahn & Pollard, 1986) and the elongation rate of actin can be affected by a single point mutation (Greve et al., 2024). Furthermore, the identical off-rate constant k_{off}^{ATP} indicates that the binding energy of the terminal subunit is very close to that of a muscle actin filament barbed end, in spite of the differences in the residues that mediate this binding (Figure 4A). *In vivo*, however, the actin filaments would not elongate at the same rate, in particular because of differences in temperature between these organisms. This suggests that the tremendous constraints that have kept these rates nearly identical over a billion years of evolution do not simply reflect the biological role of actin filaments in cells. Future studies should help determine the contributions of physiological and chemical factors in constraining these rates. For example, it would be interesting to know if purified actin filaments from other species also elongate at the same rate at 25°C. Experiments in that direction should benefit from the recent tools we have used, in particular the use of fluorescently labeled ATP to monitor the filaments. As already reported (McKane et al., 2006; Gressin et al., 2015), actin from yeast and actin from rabbit muscle can copolymerize to form hybrid filaments. Here, we find that these hybrid filaments elongate

slower, suggesting that the bonds between subunits from different species are weaker. However, in our experimental conditions, these mixed-species interfaces did not appear particularly fragile (Figure S2C-D).

In contrast to elongation, we found that yeast actin filaments depolymerize markedly faster, both in ADP·Pi- and ADP-actin, compared to mammalian filaments. Amino acid differences found in both yeast actins compared to mammals (residues marked in yellow in Figure 4A), could contribute to a weaker binding of the subunits, in particular isoleucine 43 (valine in mammals) which is located in the D-loop. By comparing recombinant and native actins for both *S. cerevisiae* and mammals, we verified that the differences in depolymerization did not come from potential post-translational modifications (Figure S5). We also verified that increasing the temperature did not affect the ranking of the different actins in terms of depolymerization rate (Figure S6).

Yeast actin filaments also release inorganic phosphate (Pi) much faster than mammalian actin filaments, and this is largely due to the absence of methylation of histidine 73 in yeast (shown in green in Figure 4A). While mammalian alpha-skeletal and beta actins are both methylated on histidine 73, the observation that the latter releases Pi 2.5-fold faster (Schahl et al., 2025) suggests that other residues are involved in this process. A good candidate is methionine 16 (shown in pink in Figure 4A), found in the nucleotide-binding pocket of yeast actins and mammalian beta but not alpha-skeletal actin (leucine16, instead), and already suggested to favor Pi release based on structural data (Stevenson et al., 2025). The importance of histidine 73 methylation highlights the need to control key post-translational modifications *in vitro*, and one should note that recombinant actins expressed in insect cells are likely to be artificially histidine 73-methylated. In *S. pombe* actin, the methylation of histidine 73 increases the affinity of Pi for the actin subunit at the barbed end (Figure 4C) without affecting its off-rate constant (k_r^{BE}, Figure 4D), and thus increases the on-rate constant of Pi into the barbed end subunit. Histidine 73 methylation also slows down the depolymerization of ADP·Pi-actin (Figure 4C, Table 3).

The release of Pi from the barbed end is also faster in yeast than in mammals, but this effect does not seem related to the absence of histidine 73 methylation in yeast (Figure 4D, Table 3). Instead, it is likely due to larger fluctuations of the terminal subunit in yeast, which may ease the opening of the Pi escape route (the so-called “back door”; Oosterheert et al., 2023; Wriggers & Schulten, 1999) or allow another route through which the Pi can escape. In the monomeric form, both yeast actins have been reported to exchange their nucleotide faster than mammalian actins (Chen et al., 1993; Ti & Pollard, 2011), and our observations using ATP-atto488 are consistent with this (Fig S7).

The cytoskeleton is particularly interesting to study in the light of evolution because it serves essential functions in diverse organisms across the tree of life. For example, actin filaments purified from apicomplexans and from *Leishmania*, which are evolutionary very far from metazoans, appear to depolymerize rapidly *in vitro* (Lu et al., 2019; Kotila et al., 2022; Hvorecny et al., 2024). This is commonly interpreted as a means for these organisms to have actin cytoskeletons that turn over very fast, in spite of having a limited set of regulatory proteins to accelerate their disassembly. *S. pombe* and *S. cerevisiae*, which are closer to metazoans, provide a somewhat intermediate situation allowing us to test and expand this interpretation. They also have very dynamic actin cytoskeletons but they have orthologs of the key ABPs found in metazoans (Moseley & Goode, 2006). The rapid depolymerization rates we report here, compared to mammalian actin filaments, could be a means for yeasts to operate efficiently at lower temperatures. The rapid Pi-release rates we measured could be important for yeasts to operate with high cytosolic concentrations of Pi (van Eunen et al., 2010). Also, since yeasts have fewer different actin networks than animal cells, they may not need such a wide range of turnover rates and may thus benefit from having less stable actin filaments. The elongation of actin filaments can be regulated by several factors in yeast cells (Billault-Chaumartin et al., 2022; Gonzalez Rodriguez et al., 2023; Homa et al., 2021; Scott et al., 2011). Nonetheless, the rates we report here indicate that, with an estimated 4 µM of actin monomers in the cytosol of *S. cerevisiae* (Gonzalez Rodriguez et al., 2023), actin filaments on their own would elongate at roughly 100 nm/s at 25°C, which appears compatible with the fast internalization observed at endocytic sites, for example (Kaksonen et al., 2005).

Yeast, and in particular *S. pombe* and *S. cerevisiae*, are powerful model organisms to study the actin cytoskeleton. Conveniently, they possess a few, well-defined and well-characterized actin networks (Kovar et al., 2011; Mishra et al., 2014), which can be studied to derive universal properties of the actin cytoskeleton. As already highlighted years ago (Berro et al., 2010; Pollard & Berro, 2009; Pollard & De La Cruz, 2013), taking full advantage of these systems requires knowing the underlying reaction rates. Here, we provide a number of essential rates that were missing (Figure S3, Table 3) and should contribute to improving our understanding of actin network dynamics in yeasts. Nonetheless, several important reaction rates remain unknown, regarding the interactions of actin filaments and monomers with ABPs in yeast. Since actin-ABP interactions can be very species-specific (Ghasemi et al., 2024; Kotila et al., 2022), future *in vitro* studies will have to carefully match the origins of the proteins in order to reliably decipher the regulation of actin dynamics.

Author contributions

IBC, GRL and AJ conceived the project. HW performed and quantified part of the experiments in Figure S5 and developed the code used to quantify experiments relative to Pi-release rate. IBC performed all other experiments and quantifications. AG purified the native yeast actin used in Figure S5. HW purified the mammalian actins used in Figure S5. IBC purified all other proteins. AM, AJ and GRL acquired funding. IBC and GRL wrote the first draft of the manuscript, which was revised by all authors.

Acknowledgments

We thank Mohan Balasubramanian for *P. pastoris* strains and plasmids, the Protéoseine facility for mass spectrometry analysis and Sophie Martin for comments on the manuscript. We acknowledge funding from Fondation pour la Recherche Médicale (grant EQU202203014630 to G.R.L.), from the Fondation Bettencourt-Schueller (grant Impulscience to A.J.), from the National Research Foundation (NRF) Singapore under its Mid-Sized Grant (MSG) (NRF-MSG-2023-0001 to A.M.) and from the National University of Singapore through the Mechanobiology Institute (A-0003467-00-00 to A.M.).

Tables

	A. thaliana	*O. cunigulus*	*S. pombe*	*S. cerevisiae*
A. thaliana	100.0	87.80	87.47	83.47
O. cunigulus	87.80	100.0	88.80	86.67
S. pombe	83.47	88.80	100.0	89.60
S. cerevisiae	83.47	86.67	89.60	100.0

Table 1. Pairwise sequence identity of the actin sequences considered in Figure 1A

	N-terminal Acetylation	His73 methylation	References
O. cunigulus	+	+	(Gaetjens & Barany, 1966; Kalhor et al., 1999)
S. pombe	+	-	(Cook et al., 1991; Kalhor et al., 1999)
S. cerevisiae	+	-	(Cook et al., 1991; Kalhor et al., 1999)

Table 2. *In vivo* presence of the two major actin PTMs in relevant actins

Constant	Reaction (Figure S3)	Actin Type	Value	Source
k_{on}^{ATP}	(1)	*Oc*ACTA1	11.6±1.2 $s^{-1}.\mu M^{-1}$	(Pollard, 1986)
		*Sp*Act1	11.6±0.7 $s^{-1}.\mu M^{-1}$	This study
		*Sc*Act1	10.0±0.7 $s^{-1}.\mu M^{-1}$	This study
		*Sp*Act1^{H73me}	11.7±0.7 $s^{-1}.\mu M^{-1}$	This study
k_{off}^{ATP}	(2)	*Oc*ACTA1	1.4±0.8 $s^{-1}.\mu M^{-1}$	(Pollard, 1986)
		*Sp*Act1	1.51±0.47 s^{-1}	This study
		*Sc*Act1	0.97±0.52 s^{-1}	This study
		*Sp*Act1^{H73me}	1.09±0.55 s^{-1}	This study
$k_{off}^{ADP \cdot Pi}$	(3)	*Oc*ACTA1	0.16±0.07 s^{-1}	(Jégou et al., 2011)
		*Sp*Act1	6.39±0.93 s^{-1}	This study
		*Sc*Act1	2.73±0.13 s^{-1}	This study
		*Sp*Act1^{H73me}	2.77±0.08 s^{-1}	This study
k_{off}^{ADP}	(4)	*Oc*ACTA1	10.4±0.5 s^{-1}	(Wioland et al., 2019)
		*Sp*Act1	27.4±1.4 s^{-1}	This study
		*Sc*Act1	30.6±0.9 s^{-1}	This study
		*Sp*Act1^{H73me}	29.1±0.8 s^{-1}	This study
k_r	(5)	*Oc*ACTA1	0.0068±0.0021 s^{-1}	(Jégou et al., 2011)
		*Sp*Act1	0.159±0.058 s^{-1}	This study
		*Sc*Act1	0.583±0.127 s^{-1}	This study
		*Sp*Act1^{H73me}	0.0277±0.0022 s^{-1}	This study
		*Oc*ACTA1	1.8±0.6 s^{-1}	(Jégou et al., 2011)

k_r^{BE}	(6)	*Sp*Act1	7.80±4.11 s^{-1}	This study
		*Sc*Act1	4.42±2.87 s^{-1}	This study
		*Sp*Act1^{H73me}	8.46±0.73 s^{-1}	This study
L_p	-	*Oc*ACTA1	9.59±0.59 µm	This study
		*Sp*Act1	8.48±0.81 µm	This study
		*Sc*Act1	7.46±0.76 µm	This study
		*Sp*Act1^{H73me}	8.52±0.76 µm	This study

Table 3. Results Summary

For all reaction rates measured in this study, the indicated values are means ± standard deviations (over N≥4 repeats), except (1) and (2) which result from a linear fit and indicate the 95% confidence interval. See Figure S3 for a scheme explaining the different reaction rates.

References

Berro, J., Sirotkin, V., & Pollard, T. D. (2010). Mathematical modeling of endocytic actin patch kinetics in fission yeast: Disassembly requires release of actin filament fragments. *Molecular Biology of the Cell*, *21*(16), 2905–2915. https://doi.org/10.1091/mbc.E10-06-0494

Billault-Chaumartin, I., Michon, L., Anderson, C. A., Yde, S. E., Suarez, C., Iwaszkiewicz, J., Zoete, V., Kovar, D. R., & Martin, S. G. (2022). Actin assembly requirements of the formin Fus1 to build the fusion focus. *Journal of Cell Science*, *135*(13), jcs260289. https://doi.org/10.1242/jcs.260289

Blanchoin, L., & Pollard, T. D. (1999). Mechanism of interaction of Acanthamoeba actophorin (ADF/Cofilin) with actin filaments. *The Journal of Biological Chemistry*, *274*(22), 15538–15546. https://doi.org/10.1074/jbc.274.22.15538

Blanchoin, L., & Pollard, T. D. (2002). Hydrolysis of ATP by Polymerized Actin Depends on the Bound Divalent Cation but Not Profilin. *Biochemistry*, *41*(2), 597–602. https://doi.org/10.1021/bi011214b

Boiero Sanders, M., Antkowiak, A., & Michelot, A. (2020). Diversity from similarity: Cellular strategies for assigning particular identities to actin filaments and networks. *Open Biology*, *10*(9), 200157. https://doi.org/10.1098/rsob.200157

Boiero Sanders, M., Toret, C. P., Guillotin, A., Antkowiak, A., Vannier, T., Robinson, R. C., & Michelot, A. (2022). Specialization of actin isoforms derived from the loss of key interactions with regulatory factors. *The EMBO Journal*, *41*(5), e107982. https://doi.org/10.15252/embj.2021107982

Buzan, J. M., & Frieden, C. (1996). Yeast actin: Polymerization kinetic studies of wild type and a poorly polymerizing mutant. *Proceedings of the National Academy of Sciences*, *93*(1), 91–95. https://doi.org/10.1073/pnas.93.1.91

Cai, L., Makhov, A. M., & Bear, J. E. (2007). F-actin binding is essential for coronin 1B function in vivo. *Journal of Cell Science*, *120*(Pt 10), 1779–1790. https://doi.org/10.1242/jcs.007641

Casella, J. F., Maack, D. J., & Lin, S. (1986). Purification and initial characterization of a protein from skeletal muscle that caps the barbed ends of actin filaments. *The Journal of Biological Chemistry*, *261*(23), 10915–10921.

Ceron, R. H., Carman, P. J., Rebowski, G., Boczkowska, M., Heuckeroth, R. O., & Dominguez, R. (2022). A solution to the long-standing problem of actin expression and purification. *Proceedings of the National Academy of Sciences*, *119*(41), e2209150119. https://doi.org/10.1073/pnas.2209150119

Chen, X., Cook, R. K., & Rubenstein, P. A. (1993). Yeast actin with a mutation in the 'hydrophobic plug' between subdomains 3 and 4 (L266D) displays a cold-sensitive polymerization defect. *The Journal of Cell Biology*, *123*(5), 1185–1195. https://doi.org/10.1083/jcb.123.5.1185

Clamp, M., Cuff, J., Searle, S. M., & Barton, G. J. (2004). The Jalview Java alignment editor. *Bioinformatics*, *20*(3), 426–427. https://doi.org/10.1093/bioinformatics/btg430

Colombo, J., Antkowiak, A., Kogan, K., Kotila, T., Elliott, J., Guillotin, A., Lappalainen, P., & Michelot, A. (2021). A functional family of fluorescent nucleotide analogues to investigate actin dynamics and energetics. *Nature Communications*, *12*(1), 548. https://doi.org/10.1038/s41467-020-20827-4

Cook, R. K., Sheff, D. R., & Rubenstein, P. A. (1991). Unusual metabolism of the yeast actin amino terminus. *The Journal of Biological Chemistry*, *266*(25), 16825–16833.

Criscuolo, A., & Gribaldo, S. (2010). BMGE (Block Mapping and Gathering with Entropy): A new software for selection of phylogenetic informative regions from multiple sequence alignments. *BMC Evolutionary Biology*, *10*(1), 210. https://doi.org/10.1186/1471-2148-10-210

D. Edelstein, A., A. Tsuchida, M., Amodaj, N., Pinkard, H., D. Vale, R., & Stuurman, N. (2014). Advanced methods of microscope control using μManager software. *Journal of Biological Methods*, *1*(2), 1. https://doi.org/10.14440/jbm.2014.36

Dohrmann, M., & Wörheide, G. (2017). Dating early animal evolution using phylogenomic data. *Scientific Reports*, *7*(1), 3599. https://doi.org/10.1038/s41598-017-03791-w

Drenckhahn, D., & Pollard, T. D. (1986). Elongation of actin filaments is a diffusion-limited reaction at the barbed end and is accelerated by inert macromolecules. *The Journal of Biological Chemistry*, *261*(27), 12754–12758.

Edelstein, A., Amodaj, N., Hoover, K., Vale, R., & Stuurman, N. (2010). Computer Control of Microscopes Using μManager. *Current Protocols in Molecular Biology*, *92*(1). https://doi.org/10.1002/0471142727.mb1420s92

Fujiwara, I., Vavylonis, D., & Pollard, T. D. (2007). Polymerization kinetics of ADP- and ADP-P_i -actin determined by fluorescence microscopy. *Proceedings of the National Academy of Sciences*, *104*(21), 8827–8832. https://doi.org/10.1073/pnas.0702510104

Funk, J., Merino, F., Venkova, L., Heydenreich, L., Kierfeld, J., Vargas, P., Raunser, S., Piel, M., & Bieling, P. (2019). Profilin and formin constitute a pacemaker system for robust actin filament growth. *eLife*, *8*, e50963. https://doi.org/10.7554/eLife.50963

Gaetjens, E., & Barany, M. (1966). N-acetylaspartic acid in G-actin. *Biochimica et Biophysica Acta (BBA) - General Subjects*, *117*(1), 176–183. https://doi.org/10.1016/0304-4165(66)90164-4

Ghasemi, F., Cao, L., Mladenov, M., Guichard, B., Way, M., Jégou, A., & Romet-Lemonne, G. (2024). Regeneration of actin filament branches from the same Arp2/3 complex. *Science Advances*, *10*(4), eadj7681. https://doi.org/10.1126/sciadv.adj7681

Gonzalez Rodriguez, S., Wirshing, A. C. E., Goodman, A. L., & Goode, B. L. (2023). Cytosolic concentrations of actin binding proteins and the implications for in vivo F-actin turnover. *Journal of Cell Biology*, *222*(12), e202306036. https://doi.org/10.1083/jcb.202306036

Goode, B. L. (2002). Purification of yeast actin and actin-associated proteins. In *Methods in Enzymology* (Vol. 351, pp. 433–441). Elsevier. https://doi.org/10.1016/S0076-6879(02)51862-0

Gouy, M., Guindon, S., & Gascuel, O. (2010). SeaView Version 4: A Multiplatform Graphical User Interface for Sequence Alignment and Phylogenetic Tree Building. *Molecular Biology and Evolution*, *27*(2), 221–224. https://doi.org/10.1093/molbev/msp259

Gressin, L., Guillotin, A., Guérin, C., Blanchoin, L., & Michelot, A. (2015). Architecture Dependence of Actin Filament Network Disassembly. *Current Biology*, *25*(11), 1437–1447. https://doi.org/10.1016/j.cub.2015.04.011

Greve, J. N., Schwäbe, F. V., Taft, M. H., & Manstein, D. J. (2024). Biochemical characterization of cardiac α-actin mutations A21V and D26N implicated in hypertrophic cardiomyopathy. *Cytoskeleton*, *81*(12), 815–831. https://doi.org/10.1002/cm.21852

Guindon, S., Dufayard, J.-F., Lefort, V., Anisimova, M., Hordijk, W., & Gascuel, O. (2010). New Algorithms and Methods to Estimate Maximum-Likelihood Phylogenies: Assessing the Performance of PhyML 3.0. *Systematic Biology*, *59*(3), 307–321. https://doi.org/10.1093/sysbio/syq010

Gunning, P. W., Ghoshdastider, U., Whitaker, S., Popp, D., & Robinson, R. C. (2015). The evolution of compositionally and functionally distinct actin filaments. *Journal of Cell Science*, *128*(11), 2009–2019. https://doi.org/10.1242/jcs.165563

Hatano, T., Alioto, S., Roscioli, E., Palani, S., Clarke, S. T., Kamnev, A., Hernandez-Fernaud, J. R., Sivashanmugam, L., Chapa-y-Lazo, B., Jones, A. M. E., Robinson, R. C., Sampath, K., Mishima, M., McAinsh, A. D., Goode, B. L., & Balasubramanian, M. K. (2018). Rapid production of pure recombinant actin isoforms in *Pichia pastoris*. *Journal of Cell Science*, *131*(8), jcs213827. https://doi.org/10.1242/jcs.213827

Hatano, T., Sivashanmugam, L., Suchenko, A., Hussain, H., & Balasubramanian, M. K. (2020). Pick-ya actin – a method to purify actin isoforms with bespoke key post-translational modifications. *Journal of Cell Science*, *133*(2), jcs241406. https://doi.org/10.1242/jcs.241406

Homa, K. E., Zsolnay, V., Anderson, C. A., O'Connell, M. E., Neidt, E. M., Voth, G. A., Bidone, T. C., & Kovar, D. R. (2021). Formin Cdc12's specific actin assembly properties are tailored for cytokinesis in fission yeast. *Biophysical Journal*, *120*(15), 2984–2997. https://doi.org/10.1016/j.bpj.2021.06.023

Hvorecny, K. L., Sladewski, T. E., De La Cruz, E. M., Kollman, J. M., & Heaslip, A. T. (2024). Toxoplasma gondii actin filaments are tuned for rapid disassembly and turnover. *Nature Communications*, *15*(1), 1840. https://doi.org/10.1038/s41467-024-46111-3

Jégou, A., Niedermayer, T., Orbán, J., Didry, D., Lipowsky, R., Carlier, M.-F., & Romet-Lemonne, G. (2011). Individual Actin Filaments in a Microfluidic Flow Reveal the Mechanism of ATP Hydrolysis and Give Insight Into the Properties of Profilin. *PLoS Biology*, *9*(9), e1001161. https://doi.org/10.1371/journal.pbio.1001161

Junier, T., & Zdobnov, E. M. (2010). The Newick utilities: High-throughput phylogenetic tree processing in the U NIX shell. *Bioinformatics*, *26*(13), 1669–1670. https://doi.org/10.1093/bioinformatics/btq243

Kaksonen, M., Toret, C. P., & Drubin, D. G. (2005). A Modular Design for the Clathrin- and Actin-Mediated Endocytosis Machinery. *Cell*, *123*(2), 305–320. https://doi.org/10.1016/j.cell.2005.09.024

Kalhor, H. R., Niewmierzycka, A., Faull, K. F., Yao, X., Grade, S., Clarke, S., & Rubenstein, P. A. (1999). A Highly Conserved 3-Methylhistidine Modification Is Absent in Yeast Actin. *Archives of Biochemistry and Biophysics*, *370*(1), 105–111. https://doi.org/10.1006/abbi.1999.1370

Kang, H., Bradley, M. J., McCullough, B. R., Pierre, A., Grintsevich, E. E., Reisler, E., & De La Cruz, E. M. (2012). Identification of cation-binding sites on actin that drive polymerization and modulate bending stiffness. *Proceedings of the National Academy of Sciences*, *109*(42), 16923–16927. https://doi.org/10.1073/pnas.1211078109

Katoh, K., & Standley, D. M. (2013). MAFFT Multiple Sequence Alignment Software Version 7: Improvements in Performance and Usability. *Molecular Biology and Evolution*, *30*(4), 772–780. https://doi.org/10.1093/molbev/mst010

Korn, E. D., Carlier, M. F., & Pantaloni, D. (1987). Actin polymerization and ATP hydrolysis. *Science (New York, N.Y.)*, *238*(4827), 638–644. https://doi.org/10.1126/science.3672117

Kotila, T., Wioland, H., Selvaraj, M., Kogan, K., Antenucci, L., Jégou, A., Huiskonen, J. T., Romet-Lemonne, G., & Lappalainen, P. (2022). Structural basis of rapid actin dynamics in the evolutionarily divergent Leishmania parasite. *Nature Communications*, *13*(1), 3442. https://doi.org/10.1038/s41467-022-31068-y

Kovar, D. R., Sirotkin, V., & Lord, M. (2011). Three's company: The fission yeast actin cytoskeleton. *Trends in Cell Biology*, *21*(3), 177–187. https://doi.org/10.1016/j.tcb.2010.11.001

Kurtzman, C. P. (2009). Biotechnological strains of Komagataella (Pichia) pastoris are Komagataella phaffii as determined from multigene sequence analysis. *Journal of Industrial Microbiology & Biotechnology*, *36*(11), 1435–1438. https://doi.org/10.1007/s10295-009-0638-4

Lappalainen, P., Kotila, T., Jégou, A., & Romet-Lemonne, G. (2022). Biochemical and mechanical regulation of actin dynamics. *Nature Reviews. Molecular Cell Biology*, *23*(12), 836–852. https://doi.org/10.1038/s41580-022-00508-4

Lemoine, F., Correia, D., Lefort, V., Doppelt-Azeroual, O., Mareuil, F., Cohen-Boulakia, S., & Gascuel, O. (2019). NGPhylogeny.fr: New generation phylogenetic services for non-specialists. *Nucleic Acids Research*, *47*(W1), W260–W265. https://doi.org/10.1093/nar/gkz303

Lemoine, F., Domelevo Entfellner, J.-B., Wilkinson, E., Correia, D., Dávila Felipe, M., De Oliveira, T., & Gascuel, O. (2018). Renewing Felsenstein's phylogenetic bootstrap in the era of big data. *Nature*, *556*(7702), 452–456. https://doi.org/10.1038/s41586-018-0043-0

Lu, H., Fagnant, P. M., & Trybus, K. M. (2019). Unusual dynamics of the divergent malaria parasite *Pf* Act1 actin filament. *Proceedings of the National Academy of Sciences*, *116*(41), 20418–20427. https://doi.org/10.1073/pnas.1906600116

Madeira, F., Madhusoodanan, N., Lee, J., Eusebi, A., Niewielska, A., Tivey, A. R. N., Lopez, R., & Butcher, S. (2024). The EMBL-EBI Job Dispatcher sequence analysis tools framework in 2024. *Nucleic Acids Research*, *52*(W1), W521–W525. https://doi.org/10.1093/nar/gkae241

Mazzini, V., & Craig, V. S. J. (2017). What is the fundamental ion-specific series for anions and cations? Ion specificity in standard partial molar volumes of electrolytes and electrostriction in water and non-aqueous solvents. *Chemical Science*, *8*(10), 7052–7065. https://doi.org/10.1039/C7SC02691A

McCullough, B. R., Grintsevich, E. E., Chen, C. K., Kang, H., Hutchison, A. L., Henn, A., Cao, W., Suarez, C., Martiel, J.-L., Blanchoin, L., Reisler, E., & De La Cruz, E. M. (2011). Cofilin-Linked Changes in Actin Filament Flexibility Promote Severing. *Biophysical Journal*, *101*(1), 151–159. https://doi.org/10.1016/j.bpj.2011.05.049

McKane, M., Wen, K.-K., Meyer, A., & Rubenstein, P. A. (2006). Effect of the Substitution of Muscle Actin-specific Subdomain 1 and 2 Residues in Yeast Actin on Actin Function. *Journal of Biological Chemistry*, *281*(40), 29916–29928. https://doi.org/10.1074/jbc.M602251200

Melki, R., Fievez, S., & Carlier, M.-F. (1996). Continuous Monitoring of P_i Release Following Nucleotide Hydrolysis in Actin or Tubulin Assembly Using 2-Amino-6-mercapto-7-methylpurine Ribonucleoside and Purine-Nucleoside Phosphorylase as an Enzyme-Linked Assay. *Biochemistry*, *35*(37), 12038–12045. https://doi.org/10.1021/bi961325o

Mishra, M., Huang, J., & Balasubramanian, M. K. (2014). The yeast actin cytoskeleton. *FEMS Microbiology Reviews*, *38*(2), 213–227. https://doi.org/10.1111/1574-6976.12064

Moseley, J. B., & Goode, B. L. (2006). The Yeast Actin Cytoskeleton: From Cellular Function to Biochemical Mechanism. *Microbiology and Molecular Biology Reviews*, *70*(3), 605–645. https://doi.org/10.1128/MMBR.00013-06

Nickaeen, M., Berro, J., Pollard, T. D., & Slepchenko, B. M. (2022). A model of actin-driven endocytosis explains differences of endocytic motility in budding and fission yeast. *Molecular Biology of the Cell*, *33*(3), ar16. https://doi.org/10.1091/mbc.E21-07-0362

Oosterheert, W., Blanc, F. E. C., Roy, A., Belyy, A., Sanders, M. B., Hofnagel, O., Hummer, G., Bieling, P., & Raunser, S. (2023). Molecular mechanisms of inorganic-phosphate release from the core and barbed end of actin filaments. *Nature Structural & Molecular Biology*, *30*(11), 1774–1785. https://doi.org/10.1038/s41594-023-01101-9

Perrin, B. J., & Ervasti, J. M. (2010). The actin gene family: Function follows isoform. *Cytoskeleton*, *67*(10), 630–634. https://doi.org/10.1002/cm.20475

Picco, A., Toret, C. P., Rivier-Cordey, A.-S., & Kaksonen, M. (2025). Mosaic evolution of clathrin-mediated endocytosis in fungi. *Current Biology*, *35*(15), 3674-3686.e4. https://doi.org/10.1016/j.cub.2025.06.052

Pollard, T. D. (1986). Rate constants for the reactions of ATP- and ADP-actin with the ends of actin filaments. *The Journal of Cell Biology*, *103*(6), 2747–2754. https://doi.org/10.1083/jcb.103.6.2747

Pollard, T. D., & Berro, J. (2009). Mathematical Models and Simulations of Cellular Processes Based on Actin Filaments. *Journal of Biological Chemistry*, *284*(9), 5433–5437. https://doi.org/10.1074/jbc.R800043200

Pollard, T. D., & Cooper, J. A. (2009). Actin, a central player in cell shape and movement. *Science (New York, N.Y.)*, *326*(5957), 1208–1212. https://doi.org/10.1126/science.1175862

Pollard, T. D., & De La Cruz, E. M. (2013). Take advantage of time in your experiments: A guide to simple, informative kinetics assays. *Molecular Biology of the Cell*, *24*(8), 1103–1110. https://doi.org/10.1091/mbc.e13-01-0030

Rodrigues-Oliveira, T., Wollweber, F., Ponce-Toledo, R. I., Xu, J., Rittmann, S. K.-M. R., Klingl, A., Pilhofer, M., & Schleper, C. (2023). Actin cytoskeleton and complex cell architecture in an Asgard archaeon. *Nature*, *613*(7943), 332–339. https://doi.org/10.1038/s41586-022-05550-y

Schahl, A., Lagardère, L., Walker, B., Ren, P., Wioland, H., Ballet, M., Jégou, A., Chavent, M., & Piquemal, J.-P. (2025). Histidine 73 methylation coordinates β-actin plasticity in response to key environmental factors. *Nature Communications*, *16*(1), 2304. https://doi.org/10.1038/s41467-025-57458-6

Schindelin, J., Arganda-Carreras, I., Frise, E., Kaynig, V., Longair, M., Pietzsch, T., Preibisch, S., Rueden, C., Saalfeld, S., Schmid, B., Tinevez, J.-Y., White, D. J., Hartenstein, V., Eliceiri, K., Tomancak, P., & Cardona, A. (2012). Fiji: An open-source platform for biological-image analysis. *Nature Methods*, *9*(7), 676–682. https://doi.org/10.1038/nmeth.2019

Scott, B. J., Neidt, E. M., & Kovar, D. R. (2011). The functionally distinct fission yeast formins have specific actin-assembly properties. *Molecular Biology of the Cell*, *22*(20), 3826–3839. https://doi.org/10.1091/mbc.e11-06-0492

Shen, X.-X., Steenwyk, J. L., LaBella, A. L., Opulente, D. A., Zhou, X., Kominek, J., Li, Y., Groenewald, M., Hittinger, C. T., & Rokas, A. (2020). Genome-scale phylogeny and contrasting modes of genome evolution in the fungal phylum Ascomycota. *Science Advances*, *6*(45), eabd0079. https://doi.org/10.1126/sciadv.abd0079

Šlajcherová, K., Fišerová, J., Fischer, L., & Schwarzerová, K. (2012). Multiple Actin Isotypes in Plants: Diverse Genes for Diverse Roles? *Frontiers in Plant Science*, *3*. https://doi.org/10.3389/fpls.2012.00226

Spudich, J. A., & Watt, S. (1971). The regulation of rabbit skeletal muscle contraction. I. Biochemical studies of the interaction of the tropomyosin-troponin complex with actin and the proteolytic fragments of myosin. *The Journal of Biological Chemistry*, *246*(15), 4866–4871.

Stevenson, S. R., Tzokov, S. B., Lahiri, I., Ayscough, K. R., & Bullough, P. A. (2025). Cryo-EM reconstruction of yeast ADP-actin filament at 2.5 Å resolution. A comparison with vertebrate F-actin. *Structure*, *33*(3), 435-442.e3. https://doi.org/10.1016/j.str.2024.12.008

Takaine, M., & Mabuchi, I. (2007). Properties of Actin from the Fission Yeast Schizosaccharomyces pombe and Interaction with Fission Yeast Profilin. *Journal of Biological Chemistry*, *282*(30), 21683–21694. https://doi.org/10.1074/jbc.M611371200

Tang, Q., Pollard, L. W., Homa, K. E., Kovar, D. R., & Trybus, K. M. (2023). Acetylation of fission yeast tropomyosin does not promote differential association with cognate formins. *Cytoskeleton*, *80*(3–4), 77–92. https://doi.org/10.1002/cm.21745

Ti, S.-C., & Pollard, T. D. (2011). Purification of Actin from Fission Yeast Schizosaccharomyces pombe and Characterization of Functional Differences from Muscle Actin. *Journal of Biological Chemistry*, *286*(7), 5784–5792. https://doi.org/10.1074/jbc.M110.199794

van Eunen, K., Bouwman, J., Daran-Lapujade, P., Postmus, J., Canelas, A. B., Mensonides, F. I. C., Orij, R., Tuzun, I., van den Brink, J., Smits, G. J., van Gulik, W. M., Brul, S., Heijnen, J. J., de Winde, J. H., de Mattos, M. J. T., Kettner, C., Nielsen, J., Westerhoff, H. V., & Bakker, B. M. (2010). Measuring enzyme activities under standardized in vivo-like conditions for systems biology. *The FEBS Journal*, *277*(3), 749–760. https://doi.org/10.1111/j.1742-4658.2009.07524.x

Vandekerckhove, J., & Weber, K. (1978). Actin Amino-Acid Sequences. Comparison of Actins from Calf Thymus, Bovine Brain, and SV40-Transformed Mouse 3T3 Cells with Rabbit Skeletal Muscle Actin. *European Journal of Biochemistry*, *90*(3), 451–462. https://doi.org/10.1111/j.1432-1033.1978.tb12624.x

Wilkinson, A. W., Diep, J., Dai, S., Liu, S., Ooi, Y. S., Song, D., Li, T.-M., Horton, J. R., Zhang, X., Liu, C., Trivedi, D. V., Ruppel, K. M., Vilches-Moure, J. G., Casey, K. M., Mak, J., Cowan, T., Elias, J. E., Nagamine, C. M., Spudich, J. A., … Gozani, O. (2019). SETD3 is an actin histidine methyltransferase that prevents primary dystocia. *Nature*, *565*(7739), 372–376. https://doi.org/10.1038/s41586-018-0821-8

Wioland, H., Ghasemi, F., Chikireddy, J., Romet-Lemonne, G., & Jégou, A. (2022). Using Microfluidics and Fluorescence Microscopy to Study the Assembly Dynamics of Single Actin Filaments and Bundles. *Journal of Visualized Experiments*, (183), 63891. https://doi.org/10.3791/63891

Wioland, H., Jegou, A., & Romet-Lemonne, G. (2019). Quantitative Variations with pH of Actin Depolymerizing Factor/Cofilin's Multiple Actions on Actin Filaments. *Biochemistry*, *58*(1), 40–47. https://doi.org/10.1021/acs.biochem.8b01001

Wriggers, W., & Schulten, K. (1999). Investigating a back door mechanism of actin phosphate release by steered molecular dynamics. *Proteins*, *35*(2), 262–273.

Xu, T., Langouras, C., Koudehi, M. A., Vos, B. E., Wang, N., Koenderink, G. H., Huang, X., & Vavylonis, D. (2019). Automated Tracking of Biopolymer Growth and Network Deformation with TSOAX. *Scientific Reports*, *9*(1), 1717. https://doi.org/10.1038/s41598-018-37182-6

Xu, X.-P., Cao, W., Swift, M. F., Pandit, N. G., Huehn, A. E., Sindelar, C. V., De La Cruz, E. M., Hanein, D., & Volkmann, N. (2024). High-resolution yeast actin structures indicate the molecular mechanism of actin filament stiffening by cations. *Communications Chemistry*, *7*(1), 164. https://doi.org/10.1038/s42004-024-01243-x

Yao, X., Grade, S., Wriggers, W., & Rubenstein, P. A. (1999). His73, Often Methylated, Is an Important Structural Determinant for Actin. *Journal of Biological Chemistry*, *274*(52), 37443–37449. https://doi.org/10.1074/jbc.274.52.37443

Yao, X., & Rubenstein, P. A. (2001). F-actin-like ATPase Activity in a Polymerization-defective Mutant Yeast Actin (V266G/L267G). *Journal of Biological Chemistry*, *276*(27), 25598–25604. https://doi.org/10.1074/jbc.M011797200

Zimmermann, D., Santos, A., Kovar, D. R., & Rock, R. S. (2015). Actin age orchestrates myosin-5 and myosin-6 run lengths. *Current Biology: CB*, *25*(15), 2057–2062. https://doi.org/10.1016/j.cub.2015.06.033